

Optimization and Numerical Simulation of Novel Air-cooling System for the Thermal Management of Lithium-ion Battery Pack

Xiongchao Lin^{1*}, Keke Shao^{1,2}, Caihong Wang¹

¹ School of Chemical & Environmental Engineering, China University of Mining and Technology (Beijing), D11 Xueyuan Road, Haidian District, Beijing 100083, P.R. China.

² School of Mechanical Engineering, Beijing Institute of Technology, Zhongguancun South Street, Haidian District, Beijing 100081, P.R.China

*E-mail: lxc@cumtb.edu.cn

Received: 4 September 2021 / Accepted: 12 October 2021 / Published: 6 December 2021

A thermal management system to cool the battery pack and control the operating temperature within a safe range is very essential for power battery. In this study, a staggered counterflow air-cooling structure was proposed to enhance the low heat transfer efficiency of air-cooling module in the lithium-ion battery and reduce the largely local temperature difference. The main factors (i.e., height of channel, velocity of air, and the number of channels) affecting the temperature distribution of cell were systematically investigated. Particularly, orthogonal test combined with single factor analysis method was used to optimize the thermal management system of lithium-ion battery. Such method could greatly reduce the number of tests and improve work efficiency. The results show that the maximum temperature (T_{\max}) and maximum temperature difference ($T_{\max, \text{diff}}$) of the battery gradually decreased with the increase of the height of flow channels. Higher flow rate of the cooling medium could obviously reduce the T_{\max} of the battery. The number of the flow channels presented insignificant effect on reducing the T_{\max} of the battery. The optimized parameters were height at 4 mm, velocity at 3m/s and number of channels at 6. Under the optimized condition, the battery achieved a better temperature distribution with a minimum T_{\max} and $T_{\max, \text{diff}}$.

Keywords: Air-cooling; Lithium-ion battery; Thermal management; Numerical simulation, orthogonal matrix

1. INTRODUCTION

The development of electric vehicles, including hybrid electric vehicles (HEVs) and pure electric vehicles (EVs), as well as fuel cell vehicles (FCV), have attracted widespread attentions [1]. It is well known that the power battery pack is the core of electric vehicles directly impacting the performance

and lifetime of electric vehicles [2]. A suitable working environment of the power battery pack is an important prerequisite for ensuring the safe of the battery [3].

The organic materials in the widely used lithium-ion batteries are highly sensitive to temperature [4]. Excessively low or high temperatures will significantly affect the performance and safety of the battery. Studies have shown that the best operating temperature range of lithium-ion batteries is 20~40 °C, and the maximum temperature difference ($T_{\max, \text{diff}}$) of the single cell should not exceed 5 °C [5]. On some special occasions, the working environment of battery pack usually under very harsh condition [6]. The accidentally spontaneous combustions of electric vehicles are frequently reported around the world [7]. Therefore, it is essential to equip a thermal management system to cool the battery and control the operating temperature within a safe range [8].

At present, many scholars in the world have put forward many strategies for the thermal management system of lithium-ion batteries. Battery thermal management can be classified into three categories according to different cooling media, *i.e.*, air-cooling [9], liquid-cooling [10] and phase-change material cooling [11]. Liquid-cooling has a high cooling efficiency meeting the need of high-rate charging and discharging. However, such system with extra accessory equipment seriously weakens the travel distance of electric vehicles. Phase-change materials with large phase enthalpy could maintain a constant temperature when absorbs the heat generated by the battery pack. However, its development and application were severely restricted due to the large thermal resistance and technical immature [11]. Although air-cooling has the problem of low heat exchange efficiency, its simple structure and convenient operation still have important significance and practical value. Peng et al. [12] used equivalent circuit models to investigate the impact of the position and distribution of the cooling air inlet and outlet on the temperature distribution of the battery pack. The height of the air inlet was found have obvious influence on the battery temperature. Arranging the inlet and outlet on the same side was more conducive to heat dissipation. Sun et al. [13] evaluated the Z-shaped structure of air-cooled square battery packs. By adding two secondary pipes on the opposite side of the outlet, the uniformity of the battery temperature was improved. In addition, by inserting bellows between the battery cells, the specific cooling surface area and cooling efficiency of each flow channel increased; while the temperature of the battery could be further lowered. Mahamud et al. [14] designed a reciprocating cycle air intake thermal management system, and performed a numerical analysis of the system through a lumped battery thermal model and a flow resistance network model. Shorter reciprocating intake period could achieve lower battery temperature and higher uniformity of the monomer temperature. The lumped heat model based on the heat transfer correlation was more suitable than computational fluid dynamics simulation for computing parallel battery pack models. Chen et al. [15] proposed a symmetrical air-cooling system with uneven battery spacing. It was found that the performance of symmetric system was significantly better than that of the asymmetric system. Hong et al. [16] reported a strategy to use secondary vents to improve air-cooled battery packs. The influence of the position and size of the secondary vent on the temperature of the battery pack was studied by computational fluid dynamics method. The cooling effect was improved when the secondary ventilation pipe was at the exit position. Consequently, the maximum temperature (T_{\max}) during the operation of the battery pack was reduced at least 60%.

The design of the air-cooling system mainly focuses on the proposing of a new type of cooling structure, including the location of the inlet and outlet, the fixation of a secondary air outlet or baffles, and the distribution of batteries. In this work, to improve the efficiency of heat transfer and reduce the inhomogeneous distribution of temperature and the T_{\max} of cells, a novel air-cooling structure with the air flows in the flow channel and opposite flow direction of the cooling medium in the adjacent flow channels was proposed. The factors affecting the efficiency of heat transfer, such as the number of flow height (H), the velocity of cooling medium (V) and the numbers of channel (N), were systematically studied through numerical simulation. There were three factors affecting the structural performance, and each factor possessed 5 levels. In order to find out the degree of influence of the three factors on the battery temperature distribution and make an easier numerical analysis, the orthogonal experimental method was conducted. The widely used multi-factor experimental method based on orthogonal matrix could meet the needs of structural optimization design. The $L_{25}(5^3)$ orthogonal arrays were adopted to investigate the quantization parameters according to related factors and levels. The T_{\max} and $T_{\max, \text{diff}}$ of battery packs was used as the evaluation index to optimize the parameters of the cooling structure. And a single factor analysis was also applied to determine the specific level value of each factor.

2. MODEL DESCRIPTION

A power lithium-ion battery cooling structure with the air flows in the flow channel and opposite flow direction of the medium in the adjacent flow channels was proposed. A sandwich-like biscuit structure with repeating units of a semi-square batteries and cooling structure with the cooling channels placed in the middle of the two batteries was designed. The cooling structure was composed of runners and partitions. The schematic diagram of the cooling structure of a lithium-ion battery is shown in Fig. 1. It is composed of a series of repeating units. The length, width and the thickness of battery are 151mm, 65mm and 16mm, respectively. The length and width of the cooling structure are equal to the battery size; the thickness range is from 1 to 5mm.

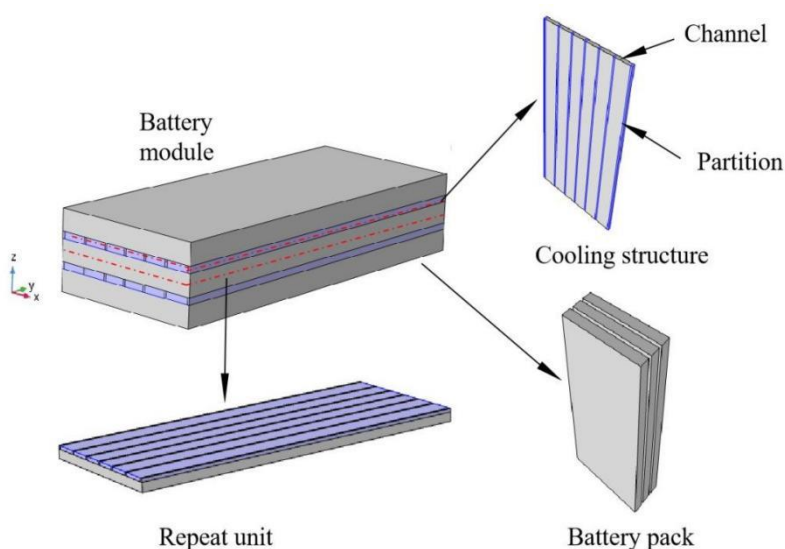


Figure 1. schematic diagram of the cooling structure of a lithium-ion battery

Fig.2 show the flow direction of the cooling medium under in channels. In order to short the calculation time, the model was simplified by regarding the battery as a uniform heating element with different thermal conductivity along the thickness and length directions. Due to the low temperature of the battery, the radiation heat exchange to the environment was ignored.

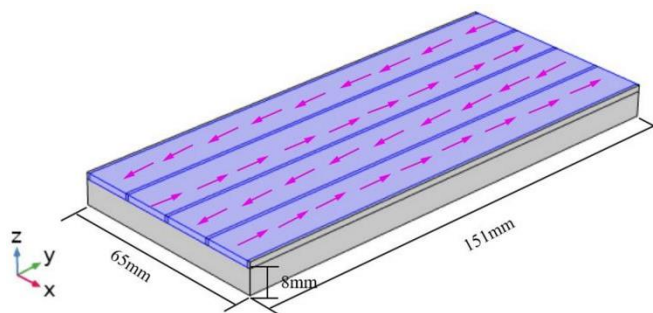


Figure 2. Flow direction of the cooling medium

2.1 Module equation and boundary condition

The cooling module can be divided into two parts, *i.e.*, heat source and the cooling structure. Heat generation and heat transfer processes mainly occur inside the battery; while, air flow and convection heat transfer correspondingly take place in the cooling structure [9].

(1) Heat generation

There are four types heat generated in battery, *i.e.*, chemical reaction (Q_r), Joule resistance (Q_J), side reaction (Q_s) and Voltage polarization (Q_p). The total generated heat of the battery (Q_t) can be thus expressed as:

$$Q_t = Q_r + Q_J + Q_s + Q_p \quad (1)$$

The heat of chemical reaction is mainly generated by the back-and-forthing movement of lithium ions between the positive and negative electrodes during the charging and discharging. The heat Q_r can be calculated as:

$$Q_r = Q / (3600 \cdot F \cdot I) \quad (2)$$

Where Q is the total chemical heat of the cell, I is the current of charge or discharge, F is the Faraday constant.

The resistor obstructing the movement of electrode material generates the Joule heat. Its computational process is:

$$Q_J = I^2 \cdot r_e \quad (3)$$

Where r_e is the resistance of electrode material.

Polarization heat is caused by the inconsistency of battery voltage and open circuit voltage when current flows through the electrodes. The Q_p can be expressed as:

$$Q_p = I^2 \cdot r_p \quad (4)$$

Where r_p represents the equivalent polarization internal resistance.

The side reaction heat is mainly generated in the abuse condition of the battery and the high temperature decomposition of the electrolyte. In the actual situation, the working temperature of the battery is strictly controlled. Therefore, this part of the heat is relatively small compared with other heat and can be ignored in the process of high-rate charge and discharge.

The heat producing rate of the battery is converted to the heat flux density, the material and heat flux boundary condition are showed in Table 1.

Table 1. medium and heat flux boundary condition [17]

Parameter	Air	Battery cell
Length (mm)	-	151.00
Width (mm)	-	65.00
Thickness (mm)	-	16.00
Density (kg/m ³)	1.18	2700.00
Dynamic viscosity (kg/(m·s))	1.98e ⁻⁵	-
Specific heat (J/(kg·K))	1003.00	900.00
Thermal conductivity (W/(m·K))	0.02	2.70/0.90
Heat source (W/m ³)	-	22845.00

(2) Heat transfer

The heat conduction in battery is expressed as [18]:

$$\rho C_p \frac{\partial t}{\partial x} = \frac{\partial}{\partial x} \left(\lambda \frac{\partial t}{\partial x} \right) + \frac{\partial}{\partial y} \left(\lambda \frac{\partial t}{\partial y} \right) + \frac{\partial}{\partial z} \left(\lambda \frac{\partial t}{\partial z} \right) + \varphi \quad (5)$$

Where ρ is density, C_p is the specific heat capacity, λ is thermal conductivity, φ is heat source.

Convection heat transfer occurs at the interface between the fluid and the battery. The process contains the momentum conservation equations, continuity equation of mass conservation, and energy conservation equations. The equations are listed as:

$$\frac{\partial u}{\partial x} + \frac{\partial v}{\partial y} = 0 \quad (6)$$

$$u \frac{\partial u}{\partial x} + v \frac{\partial u}{\partial y} = -\frac{1}{\rho} \frac{\partial p}{\partial x} + \nu \frac{\partial^2 u}{\partial y^2} \quad (7)$$

$$u \frac{\partial t}{\partial x} + v \frac{\partial t}{\partial y} = a \frac{\partial^2 t}{\partial y^2} \quad (8)$$

Where ρ is the density of air, u and v is the velocity of air, t is the temperature of cooling medium.

2.2 Grid independence test

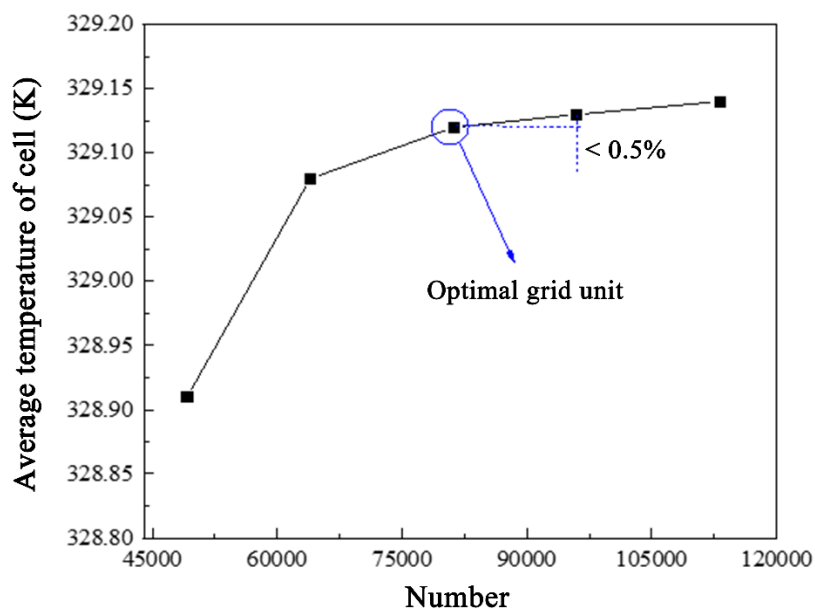


Figure 3. Grid independence test

The quality of the grid is a key factor affecting the accuracy of the numerical calculation. In order to avoid the influence of the number of grids on the numerical calculation, the independence of the grid is checked prior to the calculation. The average temperature of the battery in a natural cooling state was used as a measurement index. The five different grid number for 49205, 63960, 81185, 95940, 113160 were generated for the cooling structure, which were tested by COMSOL Multiphysics 5.4. Grid independent test results are shown in Fig. 3. It can be seen that with the number of grid elements increase, the temperature gradually elevates. When the number of grids reaches to 81185, the temperature is gradually going to less change (<0.5%). Therefore, the grid number of 81185 is used for a suitable calculation accuracy and efficiency. Each of the remaining structures is tested for grid independence before the test, until the difference between the two adjacent inspection indicators is small enough.

2.3 The flow direction of the cooling medium

In order to assess the influence of the flow direction of the cooling medium on the thermal management of the battery, the traditional single flow direction (T-S) and the staggered counterflow (S-C) of the cooling medium were compared. Their impacts on the T_{\max} , minimum temperature (T_{\min}) and $T_{\max, \text{diff}}$ of the battery was systematically investigated. The relevant results are shown in the Fig. 4. It can be seen that the T_{\max} of the battery under the two flow directions has a similar trend. The T_{\max} presents slight change with the number of flow channel increasing. In contrast, the T_{\min} in the S-C flow direction is higher than that in the T-C flow direction. And the value shows a linear relation with the number of flow channels. It is the reason for the $T_{\max, \text{diff}}$ of the battery using the S-C flow direction significantly

smaller than the T-C flow direction. Therefore, the selection of S-C flow direction has a significant advantage over T-C flow direction.

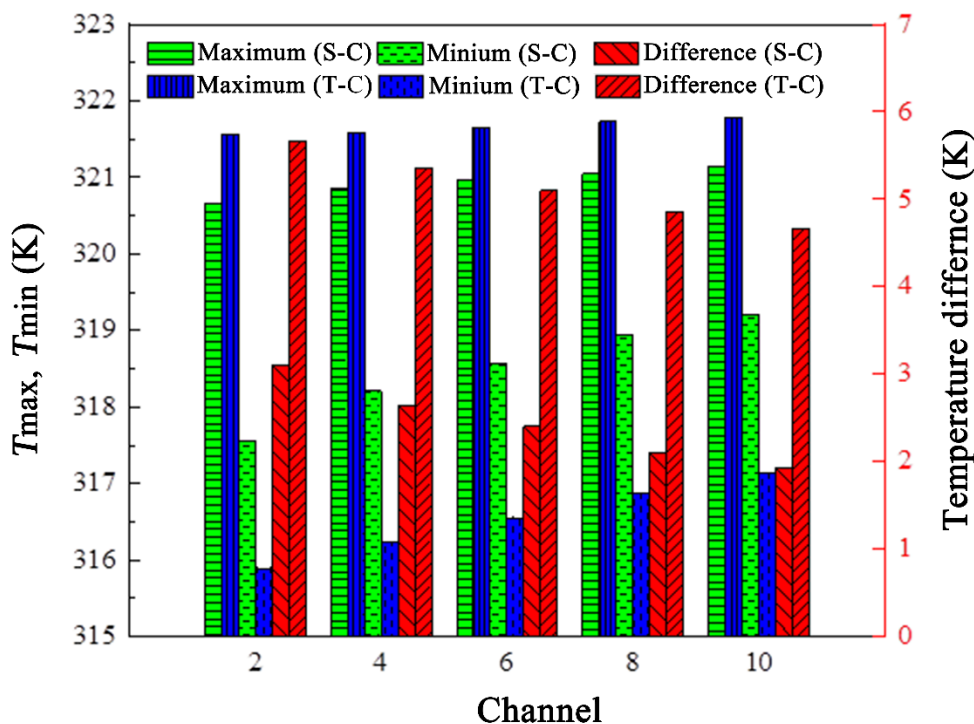


Figure 4. Influence of the flow direction

2.4 The design of orthogonal array

To explore the effects of the proposed cooling structure on the battery temperature, the T_{max} and $T_{max, diff.}$ was set as the evaluation indexes. Considering the size of the battery, the selected factors and their levels should be within a reasonable range. The factor level of the orthogonal analysis takes $5^3=125$ tests to fully expand the three-factor and five-level tests through the traditional method; while the orthogonal design method only requires 25 tests. It will greatly reduce the number of tests and short the test cycle. Therefore, the 3 factor and 5 level needed to be investigated. They were divided according to the principle of orthogonal experiment, and then filled in the L25 (5^3) orthogonal experiment table in turn [19].

3. RESULTS AND DISCUSSION

3.1 Numerical simulation

By using the COMSOL Multiphysics 5.4 software, 25 groups of different levels of combined models with typical representatives were studied and calculated. The range analysis of the T_{max} and the $T_{max, diff.}$ is shown in Table 2[20]. The X_{ct} and Y_{dt} are the sum of the Maximum temperature and

temperature difference of all orthogonal structure; $X_{ct}/5$ and $Y_{dt}/5$ are the average value of X_{ct} and Y_{dt} , where $c, d=1, 2, 3, 4, 5$ and $T=1, 2, 3, 4, 5$, respectively. Once the influence factor is determined, the difference between the average value of X_{ct} and Y_{dt} could reflect the influence of the factor on the T_{max} and $T_{max, diff.}$ of the cooling system. The range of R_c and R_d can be calculated by the formulas (9)-(12)[21].

$$S_c = \sqrt{\frac{\sum_{t=1}^5 (X_{ct} / 5 - AVE_c)^2}{6}} \tag{9}$$

$$AVE_c = \frac{1}{5} \sum_{t=1}^5 X_{ct} / 5 \tag{10}$$

$$S_d = \sqrt{\frac{\sum_{t=1}^5 (X_{dt} / 5 - AVE_d)^2}{6}} \tag{11}$$

$$AVE_d = \frac{1}{5} \sum_{t=1}^5 X_{dt} / 5 \tag{12}$$

As shown in Table 2, the height of channel (H) is the greatest impact factor among the parameters mentioned above; and the velocity of coolant (V) is the major factor impacting on the T_{max} and $T_{max, diff.}$ of cells. While, the number of channel (N) has slight impact on the indicators.

Table 2. range analysis of the T_{max} and $T_{max, diff.}$

Index	T_{max} (K)			Index	$T_{max, diff.}$ (K)		
	Factor				Factor		
	H (mm)	N	V(m/s)		H (mm)	N	V(m/s)
X_{c1}	1597.63	1564.97	1595.66	Y_{d1}	16.44	12.77	10.52
X_{c2}	1569.78	1566.33	1575.88	Y_{d2}	13.57	12.35	12.42
X_{c3}	1561.29	1562.92	1562.92	Y_{d3}	10.78	11.99	12.54
X_{c4}	1554.18	1554.26	1554.26	Y_{d4}	9.41	11.33	11.95
X_{c5}	1549.96	1548.72	1548.72	Y_{d5}	8.69	10.45	11.46
$X_{c1/5}$	319.53	312.99	319.13	$Y_{d1/5}$	3.29	2.56	2.11
$X_{c2/5}$	313.96	313.27	315.18	$Y_{d2/5}$	2.71	2.47	2.48
$X_{c3/5}$	312.26	312.58	312.58	$Y_{d3/5}$	2.16	2.40	2.51
$X_{c4/5}$	310.84	310.85	310.85	$Y_{d4/5}$	1.88	2.27	2.39
$X_{c5/5}$	309.99	309.74	309.74	$Y_{d5/5}$	1.74	2.09	2.29
R_c	9.53	3.51	9.39	R_d	1.55	1.45	0.41
S_c	3.08	1.24	3.07	S_d	0.52	0.15	0.13

3.2 Effect of the height on cooling channel

The change of T_{max} and $T_{max, diff.}$ as a function of the height of cooling structure is shown in Fig. 5. It can be seen that when the flow rate of the cooling medium and the number of flow channels are determined, the T_{max} and $T_{max, diff.}$ of the battery are greatly reduced with the increasing of height of cooling flow channel. The T_{max} reduced from 318.55K to 308.77K, and the $T_{max, diff.}$ dropped to about 2 K at $N=2$ and $V=3$ m/s (Fig.5 (a)). Likewise, the T_{max} reduced from 319.23K to 308.95K, and the $T_{max, diff.}$ dropped to about 1.7 K at $N=6$ and $V=6$ m/s (Fig.5(b)). This is due to the fact that the amount of cool

air is relatively small when the height of the flow channel is low. The air could be quickly heated to a high temperature by the battery. With the height increasing, more air would flow into the channels to better cool the battery, hence reduce the temperature of battery. The decrease of $T_{\max, \text{diff}}$ is ascribed to the use of the special designed flow direction of the cooling medium. The heat transfer could mutually take place with the cooling medium via adjacent flow channel. In addition, it can be found that the decrease trend of T_{\max} and $T_{\max, \text{diff}}$ as a function of the channel height became gradually abated. The temperature uniformity of the battery could be improved by increasing the distance between the batteries; however, an excessively large distance will occupy a larger volume and reduce the volumetric energy density of the battery pack [22-23]. Therefore, in order to ensure the heat exchange efficiency and energy density of the stake, the height of 4 mm is appropriate.

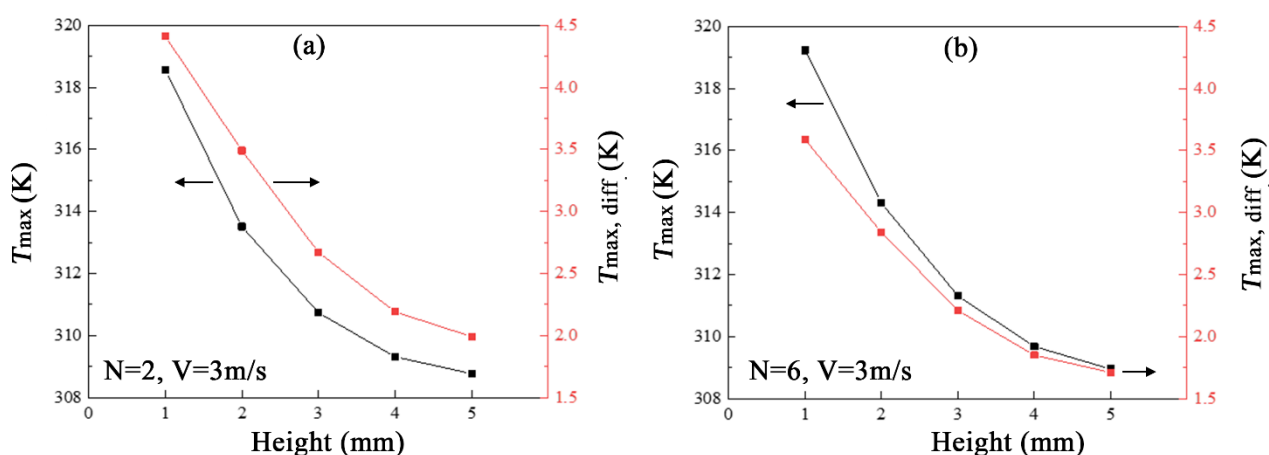


Figure 5. Effect of the height on the T_{\max} and $T_{\max, \text{diff}}$ of the cell

3.3 Effect of air velocity on the temperature distribution

It can be seen from Fig. 6 that the T_{\max} of the cell as a function of velocity of cooling medium shows decrease tendency; while, the $T_{\max, \text{diff}}$ changes in parabola form with the velocity increasing. The peak value of the $T_{\max, \text{diff}}$ appears at 2 m/s in all modes. The T_{\max} of the battery decreases from 320.66 K to 309.46 K and 320.96 K to 310.34 K at N=2 and N=6, respectively. The flow rate of the cooling medium exhibits completely different effect on the T_{\max} and $T_{\max, \text{diff}}$ of the battery. Nevertheless, it seems have little relation with the number and height of cooling channel. It was considered that the air flow rate was quite low in the channel, the extra-long residence gave rise to the adequately heat transfer between the cell and cooling medium. Consequently, the temperature difference of the battery became small. As the flow rate increases, the air residence time in the flow channel will be shortened. Only the inlet region of the battery got well cooled, thus the temperature distribution of the battery demonstrated inhomogeneous with a larger temperature difference. The continuously increase of flow rate would enhance the convective heat transfer coefficient, so as to improve the heat exchange efficiency between the battery and air. Consequently, the $T_{\max, \text{diff}}$ the battery would decrease with the increase of air flow rate. Although the temperature uniformity of the battery was able to be improved by increasing the flow

rate of the cooling medium, the battery endurance would be significantly reduced at larger air flow rates [24-25]. In addition, it can be found that the air flow channel has a greater impact on the $T_{max,diff}$ when the air flow velocity is constant. Eventually, the suitable flow rate of the cooling medium should be at least 3m/s.

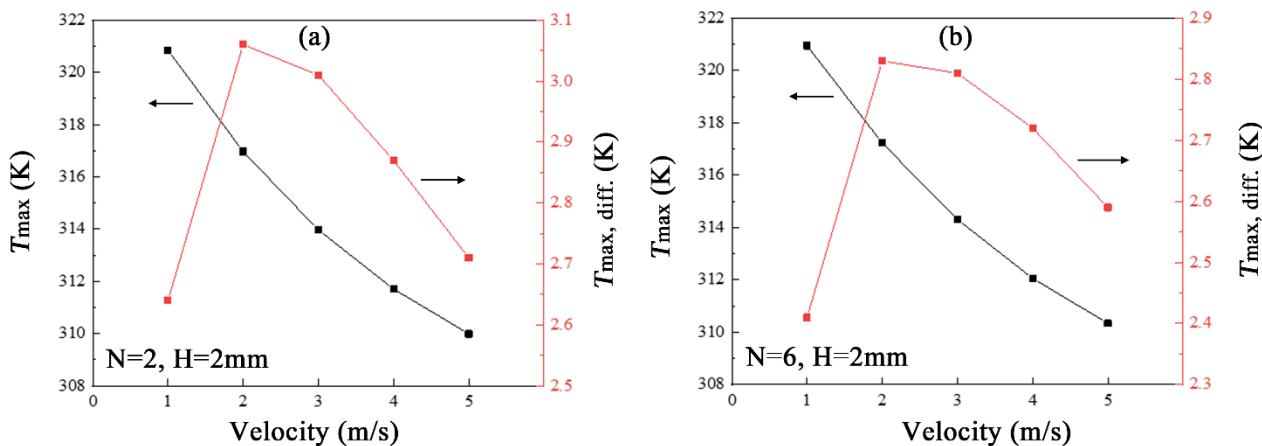


Figure 6. the change of T_{max} and $T_{max,diff}$. as a function of the cooling medium velocity

3.4 Effect of channel number on the temperature distribution

The effect of channel number on the T_{max} and $T_{max,diff}$. is shown in Fig. 7. The T_{max} of the battery tends to rise slightly, while the trends of $T_{max,diff}$. demonstrated decrease trendies with the number of channels increase. Namely, the T_{max} of the battery gradually increases from 320.66 K to 321.14 K, while the $T_{max,diff}$ greatly reduced from 3.15 K to 1.94 K with the number of cooling channels increasing from 2 to 10 at $V=1$ m/s and $H=2$ mm (Fig. 7(a)).

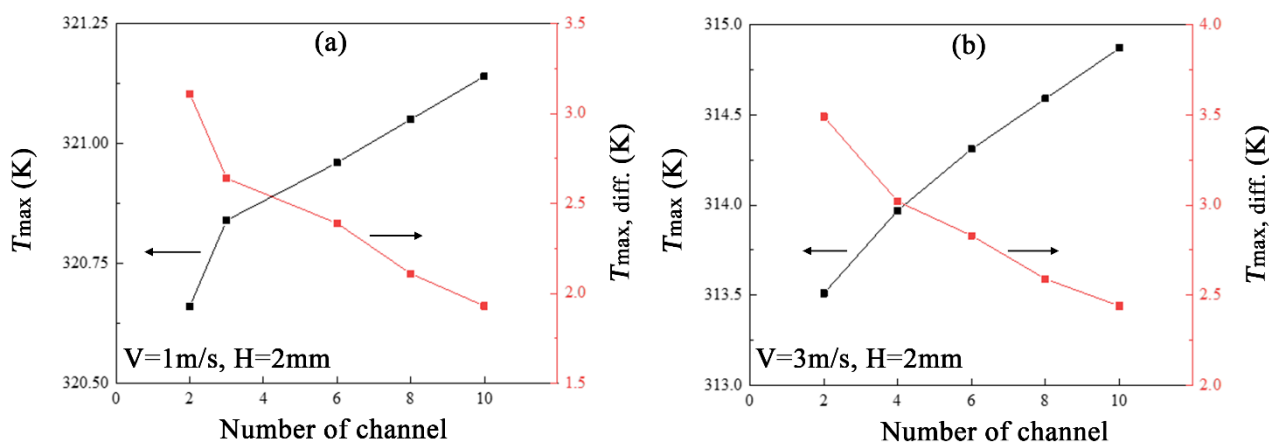


Figure 7. the effect of channel number on the T_{max} and $T_{max,diff}$.

Likewise, the T_{max} increased from 313.56 K to 314.92 K, and $T_{max,diff}$ decreased from 3.49 K to 2.52 K at $V=3$ m/s and $H=2$ mm (Fig. 7(b)). It is considered that increasing the number of cooling

channels has little effect on lowering the T_{max} , but it has greater impacts on the $T_{max,diff}$. It is because the number of partitions between the flow channels will be increased with the number of flow channels increase. And, the contact area between the cooling medium and the battery will be thus reduced. Consequently, the T_{max} of the battery gets gradually increase. In addition, the decrease of the $T_{max,diff}$ will also induce the rising of the T_{min} of the battery. Therefore, to effectively reduce the $T_{max,diff}$ of the battery, the optimized channel number in this study is 6.

From the systematically test on each condition affecting the battery temperature distribution, the optimal parameter was eventually obtained with the suitable number of channels of 6, the cooling channel height and flow channel of 4 mm, and the flow rate of cooling medium of 3 m/s (Table 3). From the comparison of temperature distribution among general conditions and selected optimal condition, the T_{max} and $T_{max,diff}$ were well optimized. Furthermore, considering the energy efficiency and manufacturing difficulty, the optimized case possesses significant advantages.

Table 3. Comparison of temperature distribution among general cases and optimized condition

Cases	H(mm)	N	V(m/s)	T_{max} (K)	$T_{max,diff}$ (K)
13	3	6	5	307.87	1.94
17	2	8	5	306.91	1.89
20	5	8	3	310.01	1.66
21	1	10	5	306.75	1.89
23	3	10	2	311.15	1.75
24	4	10	3	308.98	1.61
25	5	10	4	307.61	1.52
Optimal condition	4	6	3	309.68	1.84

Table 4. Assessment of cooling strategies for different flow directions of prismatic batteries pack [18]

Unidirectional air flow						
Cell Number	Module structure	Airflow	Spacing (mm)	T_{max} (°C)	$T_{max,diff}$ (°C)	Ref.
5	Straight	3.96 m ³ h ⁻¹	9.5	37	-	[26]
8	U-type	0.7 ms ⁻¹	4	35.7	-	[27]
8	I-type	10.8 m ³ h ⁻¹	3	31.7	3	[12]
8	I-type	2.5 ms ⁻¹	3	46.8	5	[28]
10	J-type	19.7 m ³ h ⁻¹	1	26.8	5	[29]
12	Z-type	43.2 m ³ h ⁻¹	3	60.6	8.8	[30]
24	Z-type	72 m ³ h ⁻¹	3	38.3	4.5	[31]
Reciprocating air flow						
12	-	5 ms ⁻¹	0	42.3	9.8	[16]
12	-	8 ms ⁻¹	0	38	2.2	[32]
18	-	0.4 ms ⁻¹	3	31.7	7.2	[33]
Counterflow air flow						
2	Straight	3 ms ⁻¹	4	36.53	1.84	This study

Various cooling strategies for different flow directions of prismatic batteries pack were assessed to verify the effectiveness of the proposed approach. Table 4 demonstrated the temperature comparison results among literatures and this study. It could be clearly found that, the smaller air flow rates were favorable to achieve the minimum value of the $T_{\max, \text{diff}}$ and the smaller T_{\max} . The counterflow air flow direction presented more significant advantages than unidirectional air flow direction and reciprocating air flow direction.

4. CONCLUSIONS

In this work, a novel cooling system with a staggered counterflow air-cooling structure was proposed to improve the low heat transfer efficiency of the lithium-ion battery air cooling module and reduce the largely local temperature difference. The orthogonal simulation was applied to optimize the designation of the partition channel. The T_{\max} and $T_{\max, \text{diff}}$ of cell were used as indicators to investigate the factors affecting the performance of cooling unit. The number of channel (N), the height of channel (H), and the velocity of coolant (V) are the main parameters affecting the temperature distribution of cell. The T_{\max} and $T_{\max, \text{diff}}$ of the battery gradually decreases with the increase of the height of flow channels. Higher flow rate of the cooling medium could obviously reduce the T_{\max} of the battery. While, the number of the flow channels presents insignificant effect on reducing the T_{\max} of the battery. The optimized parameters are height at 4 mm, velocity at 3m/s and number of channels at 6. Under the optimized condition, the battery achieved a better temperature distribution with a minimum T_{\max} and $T_{\max, \text{diff}}$. It is expected to be beneficial of providing a safe working environment for the battery under high discharging rate.

ACKNOWLEDGEMENT

The research is supported by the National Natural Science Foundation of China (21978319, 22008253, and 21406261).

NOMENCLATURE

Greek Letters

Q	heat, J
λ	thermal conductivity, $\text{W m}^{-1} \text{K}^{-1}$
F	Faraday constant, 96485C/mol
φ	heat source, J
I	current, A

Subscripts

r	resistance, Ω
r	reaction, /
ρ	density, $\text{kg}\cdot\text{m}^{-3}$
t	total, /
c_p	specific heat capacity, $\text{J}\cdot\text{kg}^{-1}\cdot\text{K}^{-1}$
J	Joule, /
V	X-velocity, m s^{-1}
s	side, /
U	Y-velocity, m s^{-1}
p	polarization, /
t	temperature, K
e	electrode, /

References

1. C. Q. Qiu, G. L. Wang, *Energy Convers. Manage.*, 119 (2016) 389.
2. J. T. Zhao, Z. H. Rao, Y. T. Huo, X. J. Liu and Y. M. Li, *Appl. Therm. Eng.*, 12 (2017) 33.
3. S. B. Sarmah, P. Kalita, B. Das, A. Garg, L. Gao, R. K. Pai and M. Sarma, *Int. J. Green Eng.*, 17(2020) 510.
4. D. Dan, C. N. Yao, Y. J. Zhang, H. Zhang, Z.Z. Zeng and X.M. Xu, *Appl. Therm. Eng.*, 162 (2019) 114183.
5. Y. Lv, G. Liu, G. Zahng and X. Yang, *J. Power Sources*. 468 (2020) 228398.
6. W. X. Wu, S. F. Wang, W. Wu, K. Chen, S. H. Hong and Y. X. Lai, *Energy Convers. Manage.*, 182 (2019) 262.
7. J. Deng, C. Bae, J. Marcicki, A. Masias and T. Miller, *Nat. Energy*, 3 (2018) 261.
8. Z. An, L. Jia, Y. Ding, C. Dang and X. Li, *J. Therm. Sci.*, 26 (2017) 391.
9. W. Li, M. Xiao, X. Peng, A. Garg and L. Gao, *Appl. Therm. Eng.*, 147 (2019) 90.
10. D. Chen, J. Jiang, G. Kim, C. Yang and A. Pesaran, *Appl. Therm. Eng.*, 94 (2016) 846.
11. Q. C. Wang, Z. H. Rao, Y. T. Huo and S. F. Wang, *Int. J. Heat Mass Transf.* 102(2016) 9.
12. X. B. Peng, C. Ma, A. Garg, N. S. Bao and X. P. Liao, *Appl Therm. Eng.*, 153 (2019) 596.
13. H. G. Sun, R. Dixon, *J. Power Sources*, 272 (2014) 404.
14. R. Mahamud, C. W. Park, *J. Power Sources*, 196 (2011) 5685.
15. K. Chen, Y. M. Chen, Y. Q. She, M. X. Song, S. F. Wang and L. Chen, *Appl. Therm. Eng.*, 116 (2020) 114679.

16. S. H. Hong, X. Q. Zhang, C. Kai and S. F. Wang, *Int. J. Heat Mass Transfer*, 116 (2018) 1204.
17. P Heesung, *J. Power Sources*, 239 (2013) 30.
18. D. K. Sharma, A. Prabhakar, *J. Energy Storage*, 41 (2021) 102885.
19. J.Q. E, D. D. Han, A. Qu, H. Zhu. Y. W. Deng, J. W. Chen, X. H. Zhao, W. Zuo, H. C. Wang and Q. G. Peng, *App. Therm. Eng.*, 132 (2018) 508.
20. Y. P. Liu, C. C. Ouyang, Q. B. Jiang and B. Liang, *J. Cent. South Univ.*, 22 (2015) 3970.
21. Z. Z. Shang, H. Z. Qi, X. T. Liu, C. Z. Ouyang, Y. S. Wang, *Int. J. Heat Mass Transfer*, 130 (2019) 33.
22. Y. W. Wang, J. M. Jiang, Y. H. Chung, W. C. Chen and C. M. Shu, *J. Therm. Anal. Calorim.*, 135 (2019) 2891.
23. T. Wang, K. J. Tseng, J. Y. Zhao, Z. B. Wei, *Appl. Energy*, 134 (2014) 229.
24. W. Tong, K. Somasundarm, E. Birgersson, Arun S. Mujumdar, C. Yap, *Appl. Therm. Eng.*, 99 (2016) 672.
25. Y. Yang, L. Chen, L. J. Yang, X. Z. Du, *Int. J. Therm. Science*, 165 (2021) 106968.
26. M. R. Giuliano, A. K. Prasad and S. G. Advani, *J. Power Sources*, 216 (2012) 345.
27. X.P. Liao, C. Ma, X.B. Peng, A. Garg and N. S. Bao, *J. Electrochem. Energy Convers. Storage*, 16 (2019).
28. J. J. Zhang, X. L. Wu, K. Chen, D. Zhou and M. X. Song, *J. Power Sources*, 490 (2021) 229539.
29. Y.Z. Liu, J. Zhang. *Appl. Energy*, 252 (2019) 113426.
30. K. Chen, Y. M. Chen, Z. Y. Li, F. Yuan and S. F. Wang, *Int. J. Heat Mass Transfer*, 127 (2018) 393.
31. K. H. Yu, X. Yang, Y. Z. Cheng and C. H. Li, *J. Power Sources*, 270 (2014) 193.
32. X. L. Zhang, M. Li, Y. L. Wang, F. Wang and K. Wu, *J. Energy Eng.*, 114 (2018) 4018039.
33. H. T. Wang, L. Ma, *Int. J. Heat Mass Transfer*, 115 (2017) 296.

© 2022 The Authors. Published by ESG (www.electrochemsci.org). This article is an open access article distributed under the terms and conditions of the Creative Commons Attribution license (<http://creativecommons.org/licenses/by/4.0/>).